Joint stiffness identification of six-revolute industrial serial robots

Claire Dumas *, Stéphane Caro, Sébastien Garnier, Benoît Furet

Institut de Recherche en Communications et Cybernétique de Nantes, UMR CNRS no. 6597, 1 rue de la Noë, 44321 Nantes, France

ARTICLE INFO

ABSTRACT

Although robots tend to be as competitive as CNC machines for some operations, they are not yet widely used for machining operations. This may be due to the lack of certain technical information that is required for satisfactory machining operation. For instance, it is very difficult to get information about the stiffness of industrial robots from robot manufacturers. As a consequence, this paper introduces a robust and fast procedure that can be used to identify the joint stiffness values of any six-revolute serial robot. This procedure aims to evaluate joint stiffness values considering both translational and rotational displacements of the robot end-effector for a given applied wrench (force and torque). In this paper, the links of the robot are assumed to be much stiffer than its actuated joints. The robustness of the identification method and the sensitivity of the results to measurement errors and the number of experimental tests are also analyzed. Finally, the actual Cartesian stiffness matrix of the robot is obtained from the joint stiffness values and can be used for motion planning and to optimize machining operations.

1. Introduction

Serial robots are mainly used in industry for tasks that require good repeatability but not necessarily good global pose accuracy (position + orientation as defined in ISO9283) of the robot end-effector (EE). For example, these robots are generally used for pick-and-place, painting and welding operations. Nevertheless, they are now being used for machining operations, such as the trimming, deflashing, degating, sanding and sawing of composite parts, that require high precision and stiffness. Therefore, to perform these operations, the robots must show good kinematic and elastostatic performance. In this context, it appears that conventional machine tools such as the gantry CNC are still more efficient than serial robots. Therefore, it is important to pay attention to robot performance to optimize their usefulness for machining operations. Some research works discuss the following: (i) tool path optimization considering both kinematic and dynamic robot performance [1–3]; (ii) the determination of optimal cutting parameters to avoid tool chattering [3,4]; (iii) robot stiffness analysis [5]; and (iv) the determination of robot performance indices [6–10]. Robot stiffness is also a relevant performance index for robot machining [11]. Accordingly, this paper discusses the stiffness modeling of serial robots and identifies their stiffness parameters. Some stiffness models can be found in the literature for serial and parallel manipulators [12,13]; however, the identification of stiffness parameters has yet to be determined.

Two methods were presented in [14] to obtain the Cartesian stiffness matrix (CaSM) of a five-revolute robot. The first method consists of clamping all of the joints except one to measure its stiffness. The joint stiffness matrix of the robot is obtained by repeating the procedure for each revolute joint. Therefore, only five experiments are required with this method to evaluate the CaSM of the robot throughout its Cartesian workspace assuming that the stiffness of the links is known. The second method measures the displacements of the robot end-effector due to certain applied loads and evaluates the robot Cartesian stiffness matrix throughout its Cartesian workspace with some interpolations. This method provides a good approximation of the robot CaSM when many tests are performed under different robot configurations. The second method gives better results than the first. As far as the second method is concerned, all deformations are considered including those due to the joint and link flexibilities along and about all the axes. On the contrary, in the first method, the links of the robot are assumed to be rigid, and only the stiffness of the joints is considered.

This paper introduces a method to identify the joint stiffness values of any six-revolute industrial serial robot. The proposed method is based on conservative congruence transformation [15], requires few experimental tests, is easy to implement and does not require any closed-loop control or actuator currents. This method also considers both forces and moments applied on the robot end-effector. Therefore, both the translational and rotational displacements of the robot end-effector are considered. Finally, the optimal number of experimental tests and robot

* Corresponding author. Tel.: +33 2 40 37 69 54; fax: +33 2 40 37 69 30.
E-mail addresses: claire.dumas@irccyn.ec-nantes.fr (C. Dumas),
stephane.caro@irccyn.ec-nantes.fr (S. Caro),
sebastien.garnier@irccyn.ec-nantes.fr (S. Garnier),
benoit.furet@irccyn.ec-nantes.fr (B. Furet).

configurations used to perform the joint stiffness identification are given.

The Kuka KR240-2 robot is used as an illustrative example throughout the paper. Its kinematic performances are analyzed in Section 2. Its Cartesian stiffness matrix is shown in Section 3. Section 4 contains a sensitivity analysis of the Cartesian stiffness matrix of the robot to its complementary stiffness matrix and the determination of the optimal robot configurations for joint stiffness identification. The subject of Section 5 is the robustness of the proposed joint stiffness identification method with regard to measurement noise.

2. Kinematic performance of the Kuka KR240-2 robot

The kinematic chain of the Kuka KR240-2 robot is shown in Fig. 1. The sixth link carrying the operation point P is connected to the base frame $\mathcal{F}_0$ through a serial chain composed of six-revolute joints. The modified Denavit Hartenberg parameters (DHm), described in [16], are used to parameterize the robot. Then, the kinematic Jacobian matrix of the robot was obtained, and its kinetostatic performance is evaluated throughout both its joint space and Cartesian workspace.

2.1. Parameterization

As illustrated in Fig. 1, the robot is composed of seven links, denoted as $L_0, \ldots, L_6$, and six-revolute joints. Link L_0 is the base of the robot, while link L_6 is the terminal link. Joint j connects link j with link $j-1$, $j=1,\ldots,6$. Frame $\mathcal{F}_j$ attached to link j, $j=0,\ldots,6$, is defined such that:

- the $\mathbf{z}_j$ axis is along the axis of joint j;
- the $\mathbf{x}_j$ axis is along the common normal between $\mathbf{z}_j$ and $\mathbf{z}_{j+1}$. If the axes $\mathbf{z}_j$ and $\mathbf{z}_{j+1}$ are parallel, the choice of $\mathbf{x}_j$ is not unique;
- the origin O_j is the intersection of $\mathbf{z}_j$ and $\mathbf{x}_j$.

The DHm parameters of the Kuka KR240-2 robot are given in Table 1.

The Cartesian workspace of the robot is shown in Fig. 2, and its size is characterized as $A=3100$ mm, $B=3450$ mm, $C=2700$ mm, $D=1875$ mm, $E=825$ mm, and $F=1788$ mm.

2.2. Kinematic jacobian

The 6×6 kinematic Jacobian matrix $\mathbf{J}$ of the robot relates the joint rates to the twist of the end effector, namely

$$\mathbf{t} = \begin{bmatrix} \dot{\mathbf{p}} \\ \boldsymbol{\omega} \end{bmatrix} = \mathbf{J}\dot{\boldsymbol{\theta}} \tag{1}$$

$\mathbf{t}$ is its end-effector twist, which is composed of its translational velocity vector $\dot{\mathbf{p}}$ and its angular velocity vector $\boldsymbol{\omega}$ expressed in $\mathcal{F}_0$:

$$\dot{\boldsymbol{\theta}} = [\dot{\theta}_1 \ \dot{\theta}_2 \ \dot{\theta}_3 \ \dot{\theta}_4 \ \dot{\theta}_5 \ \dot{\theta}_6]^T \tag{2}$$

$\dot{\theta}_i$ is the ith actuated revolute joint rate.

2.3. Kinetostatic performance index

We understand here under *kinetostatics* the mechanical analysis of rigid-body mechanical systems moving under static, conservative conditions. Kinetostatics is thus concerned with the relations between the feasible twists — point-velocity and angular velocity — and the constraint wrenches — force and moment — pertaining to the various links of a kinematic chain [17].

Accordingly, we focus on issues pertaining to manipulability or dexterity. We understand these terms in the sense of measures of the distance to singularity, which brings us to the concept of condition number in [18,19]. Here, we adopt the *condition number* of the underlying kinematic Jacobian matrix based on the Frobenius norm as a means to quantify distances to singularity. The *condition number* $\kappa_F(\mathbf{M})$ of an $m \times n$ matrix $\mathbf{M}$ when $m \le n$, based on the Frobenius norm is defined as follows:

$$\kappa_F(\mathbf{M}) = \frac{1}{m} \sqrt{\text{tr}(\mathbf{M}^T\mathbf{M}) \ \text{tr}[(\mathbf{M}^T\mathbf{M})^{-1}]} \tag{3}$$
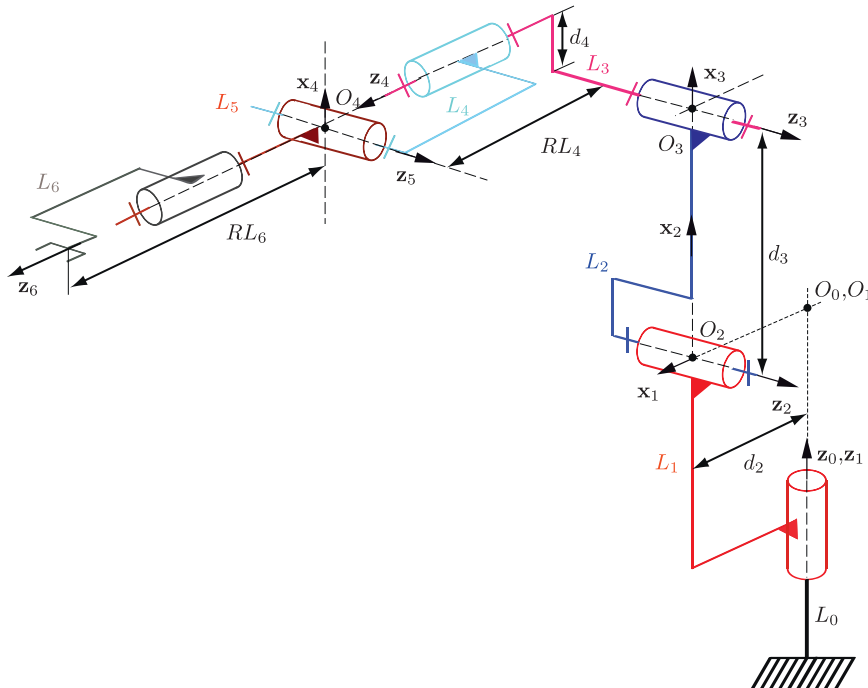

Fig. 1. DHm parameterization of the Kuka KR240-2 robot.

Here, the condition number is computed based on the Frobenius norm because the latter produces a condition number that is analytic in terms of the posture parameters, whereas the 2-norm does not. In addition, it is costlier to compute singular values than to compute matrix inverses.

The terms of matrix $\mathbf{J}$ are not homogeneous as they do not have the same units. Therefore, as shown in [20,21], the Jacobian matrix can be normalized by means of a *normalizing length*, which is called characteristic length and denoted as L. Let $\mathbf{J}_N$ be the normalized Jacobian matrix of the Kuka KR240-2 robot:

$$\mathbf{J}_N = \begin{bmatrix} \dfrac{1}{L}\mathbf{I}_{3\times3} & \mathbf{0}_{3\times3} \\ \mathbf{0}_{3\times3} & \mathbf{I}_{3\times3} \end{bmatrix}\mathbf{J} \qquad (4)$$

$\mathbf{I}_{3\times3}$ is the 3×3 identity matrix and $\mathbf{0}_{3\times3}$ is the 3×3 zero matrix. The characteristic length of the Kuka robot used in this study is equal to 0.682 m and was obtained by means of the methodology proposed in [22]. The condition number is used to have an idea of the zones (on θ_2 and θ_3 ranges) where the robot has good dexterity. It appears that a change in the condition number of $\mathbf{J}_N$ throughout the robot Cartesian workspace does not depend on L, although its value depends on L.

Because the second and the third revolute joints are the most influential joints on the translation motions of the robot end-effector, and because the first revolute joint does not affect manipulator dexterity, θ_1 is null, and the wrist angles θ_4, θ_5 and θ_6 are set to 45° so that the corresponding wrist configuration is far from singularities.

Fig. 3(a) depicts the isocontours of the inverse condition number of $\mathbf{J}_N$ based on the Frobenius norm, $\kappa_F(\mathbf{J}_N)^{-1}$, throughout the robot's Cartesian workspace. The higher the $\kappa_F(\mathbf{J}_N)^{-1}$, the better the dexterity. On the contrary, the lower the $\kappa_F(\mathbf{J}_N)^{-1}$, the closer the robot is to singularities.

Likewise, Fig. 3(b) shows the isocontours of $\kappa_F(\mathbf{J}_N)^{-1}$ throughout the robot joint space. The blacker the color, the closer the manipulator to singularities. The oblique black line characterizes the configurations in which the wrist center is located on the first joint axis. The horizontal black line in Fig. 3b characterizes the singularities when the arm is folded.
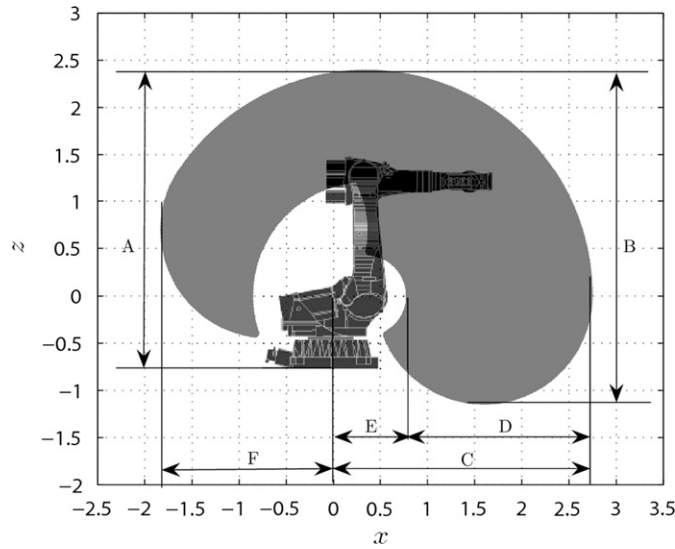
Figs. 3(a) and (b) are useful in choosing the optimal robot configurations for joint stiffness identification as explained in Section 4.

3. Cartesian stiffness matrix formulation

The Cartesian stiffness matrix of a robot depends on its configuration, link stiffness, control loop stiffness and actuators mechanical stiffness. In this paper, the last two sources of stiffness are considered. The links of the robot are assumed to

Table 1
DHm parameters of the Kuka KR240-2 robot.

j	$a(j)$	μ_j	σ_j	α_j	d_j	θ_j	r_j
1	0	1	0	0	0	θ_1	0
2	1	1	0	$\pi/2$	d_2	θ_2	0
3	2	1	0	0	d_3	θ_3	0
4	3	1	0	$-\pi/2$	d_4	θ_4	RL4
5	4	1	0	$\pi/2$	0	θ_5	0
6	5	1	0	$-\pi/2$	0	θ_6	RL6

Fig. 2. Cartesian workspace of the Kuka KR240-2 robot.
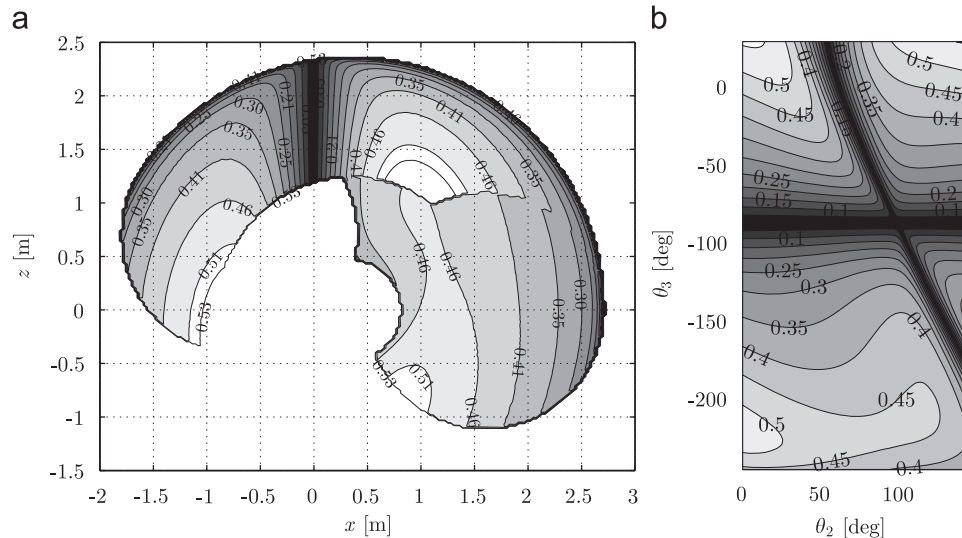
Fig. 3. Contours of the inverse condition number of $\mathbf{J}_N$: (a) in the robot Cartesian workspace and (b) in the robot joint space θ_2, θ_3.
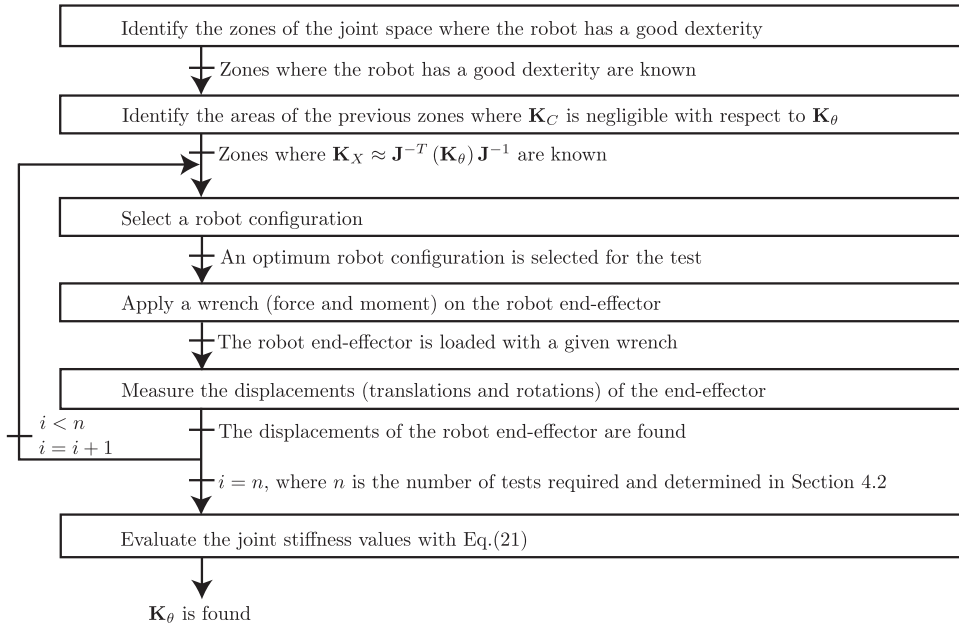
Fig. 4. Procedure for the evaluation of the joint stiffness values.

be rigid, the damping is neglected and the stiffness of the joints is represented with linear torsional springs.

Conservative congruence transformation was proposed by Chen and Kao [23] to define the spatial CaSM of a serial robot. We obtain the relation

$$w = \mathbf{K}_X \Delta X \qquad (5)$$

with

$$\mathbf{K}_X = \mathbf{J}^{-T}(\mathbf{K}_\theta - \mathbf{K}_C)\mathbf{J}^{-1} \qquad (6)$$

w is the six-dimensional wrench vector composed of the forces and torques applied on the end-effector and expressed in $\mathcal{F}_0$. $\mathbf{K}_X$ is the 6×6 CaSM of the robot expressed in $\mathcal{F}_0$. ΔX is the six-dimensional vector composed of the translational and rotational displacements of the end-effector expressed in $\mathcal{F}_0$. $\mathbf{J}$ is the kinematic Jacobian matrix of the robot defined in Eq. (1). $\mathbf{K}_\theta$ is the diagonal joint stiffness matrix defined as follows:

$$\mathbf{K}_\theta = \begin{bmatrix} k_{\theta_1} & 0 & 0 & 0 & 0 & 0 \\ 0 & k_{\theta_2} & 0 & 0 & 0 & 0 \\ 0 & 0 & k_{\theta_3} & 0 & 0 & 0 \\ 0 & 0 & 0 & k_{\theta_4} & 0 & 0 \\ 0 & 0 & 0 & 0 & k_{\theta_5} & 0 \\ 0 & 0 & 0 & 0 & 0 & k_{\theta_6} \end{bmatrix} \qquad (7)$$

where k_{θ_i}, $i = 1, \ldots, 6$, is the ith joint stiffness value. $\mathbf{K}_C$ is the complementary stiffness matrix (CoSM) defined in [15] that takes the form:

$$\mathbf{K}_C = \begin{bmatrix} \dfrac{\partial \mathbf{J}^T}{\partial \theta_1} w & \dfrac{\partial \mathbf{J}^T}{\partial \theta_2} w & \dfrac{\partial \mathbf{J}^T}{\partial \theta_3} w & \dfrac{\partial \mathbf{J}^T}{\partial \theta_4} w & \dfrac{\partial \mathbf{J}^T}{\partial \theta_5} w & \dfrac{\partial \mathbf{J}^T}{\partial \theta_6} w \end{bmatrix} \qquad (8)$$

It is noteworthy that this expression is equivalent to Salisbury's when there is no force or torque applied on the robot end-effector. Matrix $\mathbf{K}_C$ is not null and affects matrix $\mathbf{K}_X$. This expression respects the principle of virtual work and has been tested on several robots [15,24]. The identification of the joint stiffness values k_{θ_i}, $i = 1, \ldots, 6$, is the subject of the next section because they are required to evaluate $\mathbf{K}_X$ for any robot configuration.

Table 2
Arbitrary stiffness values expressed in [Nm/rad].

k_{θ_1}	k_{θ_2}	k_{θ_3}	k_{θ_4}	k_{θ_5}	k_{θ_6}
1 409 800	400 760	935 280	360 000	370 000	380 000

4. Joint stiffness matrix evaluation

Fig. 4 shows a procedure to evaluate the joint stiffness matrix $\mathbf{K}_\theta$, which was expressed in Eq. (7). First, the zones of the robot workspace and joint space where the robot has good dexterity are identified in Figs. 3(a) and (b). Then, for a given wrench applied on the robot end-effector, the areas of the previous zones where the complementary stiffness matrix $\mathbf{K}_C$ is negligible with respect to $\mathbf{K}_\theta$ are determined. Certain robot configurations are chosen from those areas for the tests. For each test, a given wrench is applied on the robot end-effector, and its displacements (translations and rotations) are measured. Finally, the joint stiffness values are obtained by a given number of tests.

4.1. Influence of $\mathbf{K}_C$ on $\mathbf{K}_X$

From Eq. (6), $\mathbf{K}_X$ depends on both $\mathbf{K}_\theta$ and $\mathbf{K}_C$. It makes sense that joint stiffness identification is easier when $\mathbf{K}_C$ is negligible with respect to $\mathbf{K}_\theta$. Consequently, this section analyzes the influence of $\mathbf{K}_C$ on $\mathbf{K}_X$. From Eq. (8), the higher the wrench applied on the robot end-effector, the higher the influence of $\mathbf{K}_C$ on $\mathbf{K}_X$. Consequently, the worst-case scenario appears when the force and the moment applied on the robot end-effector are at the maximum. Let the components of the force vector along $\mathbf{x}_0$, $\mathbf{y}_0$ and $\mathbf{z}_0$ axes be equal to 2200 N, and the components of the moment vector about $\mathbf{x}_0$, $\mathbf{y}_0$ and $\mathbf{z}_0$ axes be equal to 400 Nm. For the sake of clarity, the first three joint stiffness values are assumed to be equal to those found in [24], and the other three joint stiffness values are chosen arbitrarily as shown in Table 2.
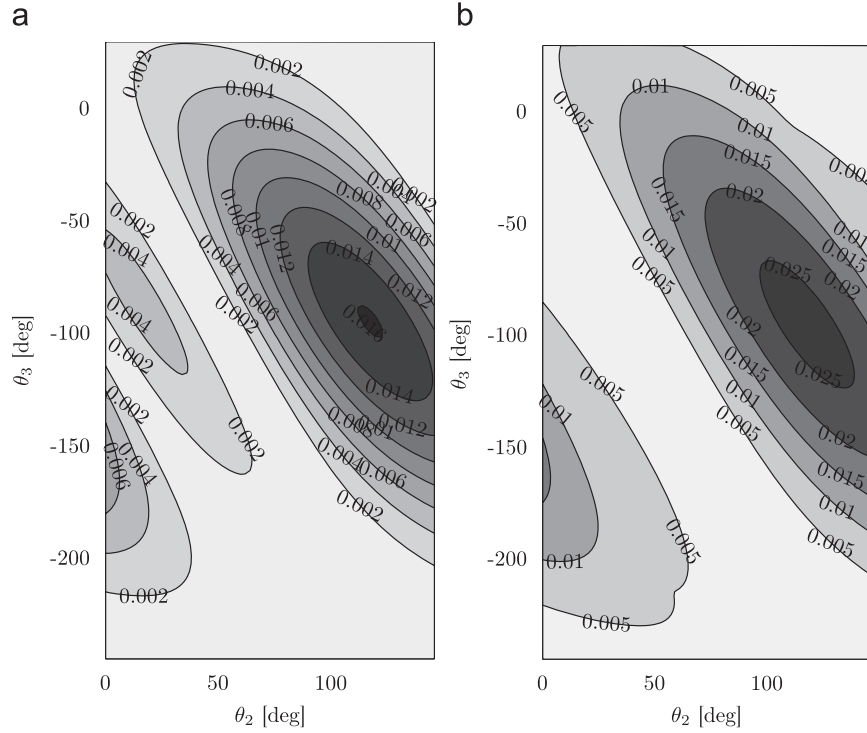
a

b

Fig. 5. Isocontours of (a) v_p and (b) v_r in the joint space (θ_2, θ_3).

The norm δp of the robot end-effector small displacement screw is expressed as

$$\delta p = \sqrt{\delta p_x^2 + \delta p_y^2 + \delta p_z^2} \tag{9}$$

where δp_x, δp_y and δp_z are its displacements along the $\mathbf{x}_0$, $\mathbf{y}_0$ and $\mathbf{z}_0$ axes, respectively. Let δr_x, δr_y and δr_z be the small rotations of the robot end-effector about $\mathbf{x}_0$, $\mathbf{y}_0$ and $\mathbf{z}_0$ axes, respectively.

Let $\delta p_{\mathbf{K}_C}$ and $\delta p_{\overline{\mathbf{K}}_C}$ be the point-displacement of the robot end-effector obtained with Eqs. (5) and (6) assuming that matrix $\mathbf{K}_C$ is not null and null, respectively. Likewise, let $\delta r_{x\mathbf{K}_C}$, $\delta r_{y\mathbf{K}_C}$, $\delta r_{z\mathbf{K}_C}$ and $\delta r_{x\overline{\mathbf{K}}_C}$, $\delta r_{y\overline{\mathbf{K}}_C}$, $\delta r_{z\overline{\mathbf{K}}_C}$ be the small rotations of the robot end-effector about the $\mathbf{x}_0$, $\mathbf{y}_0$ and $\mathbf{z}_0$ axes obtained with Eqs. (5) and (6), respectively, assuming that matrix $\mathbf{K}_C$ is not null and null, respectively.

To analyze the influence of $\mathbf{K}_C$ on $\mathbf{K}_X$ throughout the robot workspace, we introduce indices v_p and v_r, which characterize the influence of $\mathbf{K}_C$ on the evaluation of the robot translational and rotational displacements, respectively:

$$v_p = \frac{\left| \delta p_{\mathbf{K}_C} - \delta p_{\overline{\mathbf{K}}_C} \right|}{\max\left(\delta p_{\mathbf{K}_C}, \delta p_{\overline{\mathbf{K}}_C} \right)} \tag{10}$$

and

$$v_r = \max\left\{ |\delta r_{x\mathbf{K}_C} - \delta r_{x\overline{\mathbf{K}}_C}|, \ |\delta r_{y\mathbf{K}_C} - \delta r_{y\overline{\mathbf{K}}_C}|, \ |\delta r_{z\mathbf{K}_C} - \delta r_{z\overline{\mathbf{K}}_C}| \right\} \tag{11}$$

Figs. 5(a) and (b) illustrate the isocontours of v_p and v_r throughout the robot joint space (θ_2, θ_3). The blacker the color, the higher the influence of $\mathbf{K}_C$ on the evaluation of the end-effector displacements. The shapes of Fig. 5(a) and (b) are similar. This finding means that the robot configurations for which the influence of $\mathbf{K}_C$ on the end-effector translational displacements is at its maximum are the same as those for which the influence of $\mathbf{K}_C$ on the end-effector rotational displacements is at its maximum. As shown in Figs. 3(b) and 5(a) and (b), the robot configurations for which the influence of $\mathbf{K}_C$ on $\mathbf{K}_X$ are at their

maximum are also those for which $\kappa_F(\mathbf{J}_N)^{-1}$ is at its minimum, i.e., close to singularity.

Nevertheless, the v_p and v_r values are very small, $v_p \leq 0.016$ and $v_r \leq 0.025$ deg throughout the robot joint space. Accordingly, $\mathbf{K}_C$ is negligible with respect to $\mathbf{K}_\theta$, and Eq. (6) can be reduced to

$$\mathbf{K}_X \approx \mathbf{J}^{-T} \mathbf{K}_\theta \mathbf{J}^{-1} \tag{12}$$

The above-mentioned tests were conducted with different joint stiffness values than those given in Table 2. The shapes of the v_p and v_r isocontours remains the same and $\mathbf{K}_C$ remains negligible with respect to $\mathbf{K}_\theta$. Eq. (12) and the robot configurations for which v_p and v_r are at their minimum are used in the next section to identify the joint stiffness values of the robot. Then, Eq. (6) is used to evaluate the $\mathbf{K}_X$ throughout the robot Cartesian workspace for the sake of accuracy.

4.2. Identification of the joint stiffness values

For the robot configurations in which $\mathbf{K}_C$ is negligible with respect to $\mathbf{K}_\theta$, Eq. (5) takes the form:

$$\boldsymbol{w} = \mathbf{J}^{-T} \mathbf{K}_\theta \mathbf{J}^{-1} \delta \boldsymbol{d} \tag{13}$$

As a consequence, the six-dimensional robot end-effector small displacement screw $\delta \boldsymbol{d}$ can be expressed as

$$\delta \boldsymbol{d} = \mathbf{J} \mathbf{K}_\theta^{-1} \mathbf{J}^T \boldsymbol{w} \tag{14}$$

Let the joint compliances[1] be the components of the six-dimensional vector $\mathbf{x}$, namely

$$\mathbf{x} = [1/k_{\theta_1} \ \ 1/k_{\theta_2} \ \ 1/k_{\theta_3} \ \ 1/k_{\theta_4} \ \ 1/k_{\theta_5} \ \ 1/k_{\theta_6}]^T \tag{15}$$

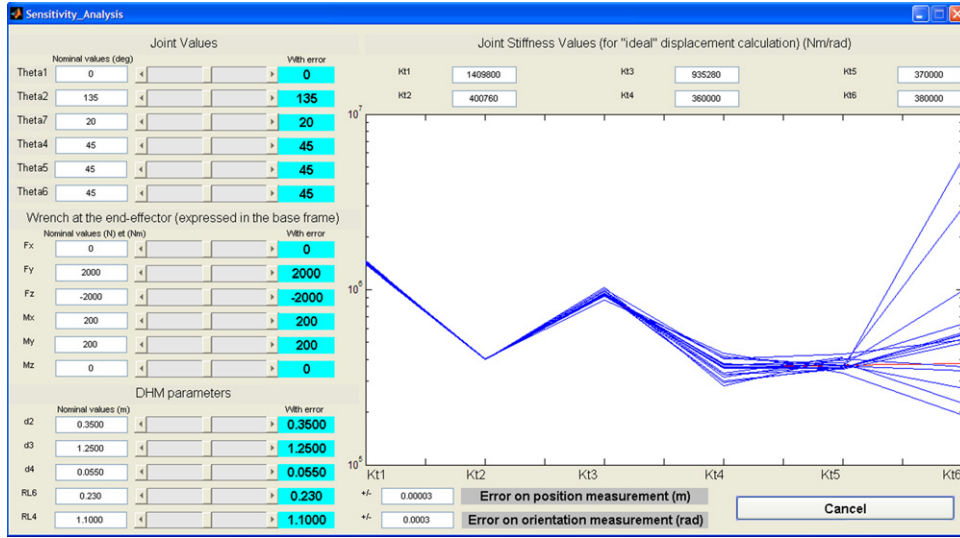[1] The compliance stands for the inverse of the stiffness.

Fig. 6. Graphical user interface—robustness of the joint stiffness identification method.

From Eq. (14), it turns out that

$$\delta\boldsymbol{d} = \begin{bmatrix} \sum_{j=1}^{6}(x_j J_{1j} \sum_{i=1}^{i=6} J_{ij} w_i) \\ \dots \\ \dots \\ \dots \\ \dots \\ \sum_{j=1}^{6}(x_j J_{6j} \sum_{i=1}^{i=6} J_{ij} w_i) \end{bmatrix} \tag{16}$$

where x_j is the jth component of vector $\mathbf{x}$, i.e., $x_j = 1/k_{\theta_j}$, $j = 1, \dots, 6$.

By isolating the components of vector $\mathbf{x}$ in Eq. (16), the joint compliances can be expressed with respect to the displacements of the robot end-effector as follows:

$$\mathbf{Ax} = \delta\boldsymbol{d} \tag{17}$$

where $\mathbf{A}$ is a 6×6 as follows:

$$\mathbf{A} = \begin{bmatrix} J_{11} \sum_{i=1}^{6} J_{i1} w_i & & & & & J_{16} \sum_{i=1}^{6} J_{i6} w_i \\ \dots & & \dots & & & \dots \\ \dots & & & \dots & & \dots \\ \dots & & \dots & & & \dots \\ \dots & & & \dots & & \dots \\ J_{61} \sum_{i=1}^{6} J_{i1} w_i & & & & & J_{66} \sum_{i=1}^{6} J_{i6} w_i \end{bmatrix} \tag{18}$$

Therefore, a six-dimensional wrench vector, a six-dimensional EE displacement vector and a 6×6 $\mathbf{A}$ matrix are associated with each test. When only one test is considered, $\mathbf{A}$ is a six-dimensional square matrix. If it is nonsingular, then Eq. (17) has a unique solution, namely

$$\mathbf{x} = \mathbf{A}^{-1}\delta\boldsymbol{d} \tag{19}$$

When several tests are considered, the equation system (17) becomes overdetermined. Assuming that n tests are considered, $n > 1$, matrix $\mathbf{A}$ becomes $6n \times 6$. Because matrix $\mathbf{A}$ is no longer square, the joint compliance vector $\mathbf{x}$ cannot be calculated using Eq. (19). Because the number of equations is higher than the number of unknowns, it is usually not possible to find a vector $\mathbf{x}$ that verifies all $6n$ equations. Accordingly, we look for the vector $\mathbf{x}$

that minimizes the following error:

$$\begin{aligned} \text{minimize } & E(\mathbf{x}) \equiv \tfrac{1}{2}\|\mathbf{Ax} - \delta d\|_2^2 \\ \text{over } & \mathbf{x} \end{aligned} \tag{20}$$

The value of $\mathbf{x}$ that minimizes the Euclidean norm of the approximation error of the system is

$$\mathbf{x}_0 = (\mathbf{A}^T\mathbf{A})^{-1}\mathbf{A}^T\delta d = \mathbf{A}^I\delta d \tag{21}$$

where $\mathbf{A}^I$ is the *generalized inverse* of $\mathbf{A}$, which is also known as the *left Moore–Penrose generalized inverse* of $\mathbf{A}$. The `Matlab` function "pinv" has been used to compute this matrix.

5. Robustness of the joint stiffness identification method with regard to measurement noise

Alici and Shirinzadeh [24] introduced a method to identify the stiffness values of the first three joints of a six-revolute robot by measuring only the translational displacements of its end-effector. Therefore, they did not considered the coupling between the rotational and translational Cartesian motions. On the contrary, our method considers both rotational and translational displacements of the end-effector, and the stiffness values of the six actuated joints can be identified as explained in the previous section. Finally, a graphical user interface (GUI), which is shown in Fig. 6, was developed to test our method and to analyze the sensitivity of the results to measurement noise.

5.1. Measurement noise

This graphical user interface requires the knowledge of the geometric and stiffness models of the robot under study. The displacements (translations and rotations) of the robot end-effector are assessed for a given wrench and given joint stiffness values. Then, assuming that the joint stiffness values are no longer known, the GUI aims at evaluating them from the end-effector displacements.

The GUI returns the exact joint stiffness values when a significant wrench is applied on the robot end-effector and when the robot does not reach any singularity. To be more realistic, the errors are considered at the identification stage. The different types of errors, which are given in Table 3, are considered and assumed to follow a normal distribution.

5.2. Optimal number of experiments

From the equation system (17), it is apparent that the higher the number of tests, the higher the degree of constraint of the equation system, the more accurate the solution.

Let us assume that the actual joint stiffness values of the robot are those given in Table 2, and the wrench applied on the robot end-effector is

$$\mathbf{w}_{eff} = \begin{bmatrix} 0\,\text{N} \\ 2200\,\text{N} \\ 2200\,\text{N} \\ 200\,\text{Nm} \\ 200\,\text{Nm} \\ 0\,\text{Nm} \end{bmatrix} \tag{22}$$

Fig. 7 illustrates the mean and standard deviation of the joint stiffness values obtained by using the proposed identification method and for different numbers of tests. From Eq. (17), matrix **A** has the size of $6n \times 6$ for n tests.

We can see that the higher the n, the lower the standard deviation of the joint stiffness values, i.e., the more accurate the evaluation of the joint stiffness values. Obviously, the higher the number of tests, the more expensive the identification of the joint stiffness values. Therefore, the user must compromise between

identification accuracy and identification cost. Fig. 7 shows that five tests are a good compromise.

5.3. Optimal robot configurations

The joint stiffness identification method is based on Eq. (21), which requires matrix **A** to be invertible. To this end, the robot configuration must be chosen such that $\kappa_F(\mathbf{J}_N)^{-1}$, where $\mathbf{J}_N$ is defined in Eq. (4), is as high as possible.

Fig. 8 depicts three zones in the joint space that were obtained from Figs. 3(a) and (b). The sensitivity of the solution of Eq. (21) to errors is at its minimum in the light gray zones. On the contrary, this sensitivity reaches its maximum in the black zones. Therefore, Table 4 gives θ_2 and θ_3 ranges associated with good robot configurations for joint stiffness identification.
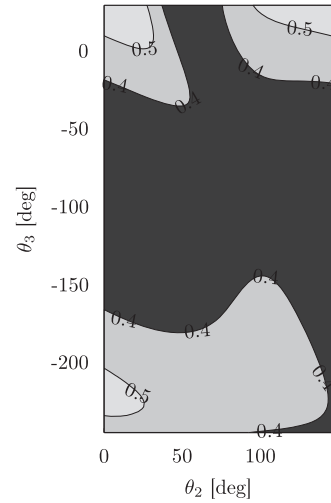

Fig. 8. Selection of robot configurations in the joint space.

Table 3
Sources of errors.

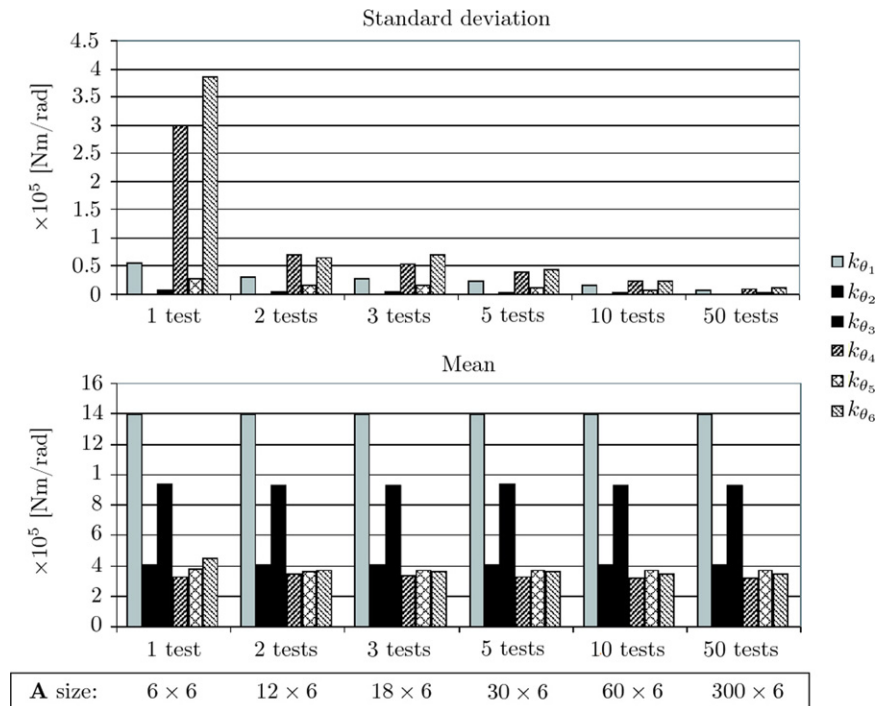| Source of errors	Magnitude ($\pm$)
Position measuring system (tracker resolution)	0.03 mm
Orientation measuring system (tracker resolution)	0.0003 rad
Geometric parameters errors (geometric calibration)	0.03 mm
Force measurement (force sensor)	0.25 N
Torque measurement (torque sensor)	0.0125 Nm
Joint angles (encoder resolution)	0.0001 rad

Fig. 7. Mean and standard deviation of the joint stiffness values as a function of the number of tests.

Table 4
Optimal robot configurations: ranges of θ_2 and θ_3.

Zone	θ_2	θ_3
1	0° to 110°	−245° to −170°
2	0° to 25°	0° to 29°
3	100° to 146°	0° to 29°

Furthermore, matrix $\mathbf{K}_C$ should be negligible for all robot configurations used for the joint stiffness identification. Thus, the light gray zones shown in Fig. 8 are correct according to Figs. 5(a) and (b).

The GUI shown in Fig. 6 allows the user to analyze the sensitivity of the results to the errors described in Table 3. The broken lines correspond to the joint stiffness values obtained with different sets of errors. We can notice that the sixth joint stiffness value, i.e., k_{θ_6}, is the most sensitive to errors because the distance between the broken lines is a maximum for this joint stiffness value. It means that the identification of k_{θ_6} is more difficult than the identification of its counterparts. This result makes sense because the initial value of k_{θ_6} given in Table 2 is higher than those of k_{θ_4} and k_{θ_5}. The first three joint stiffness values are determined correctly because the first three components of $\mathbf{w}_{eff}$ given in Eq. (22), i.e., the forces applied on the robot end-effector along the $\mathbf{x}_0$, $\mathbf{y}_0$ and $\mathbf{z}_0$ axes, are high enough to cause a significant translational displacement of the end-effector.

The user can easily check the sensitivity of the results to variations in each parameter by using the scrollbars. The lower the torque applied on the robot end-effector, the lower the standard deviations of k_{θ_i}, $i = 1, \ldots, 6$. Finally, the user must pay attention to the measurement system used to assess the end-effector orientation because the corresponding results are very sensitive to measurement noise.

6. Conclusions

The subject of this paper was to develop a new methodology for the joint stiffness identification of six-revolute industrial serial robots. A robust procedure for joint stiffness identification was proposed, and the Kuka KR240-2 robot was used as an illustrative example throughout the paper. First, the robot kinematic model was obtained to determine the optimal robot configurations according to the condition number of its kinematic Jacobian matrix. Then, its stiffness model was developed through its Cartesian stiffness matrix $\mathbf{K}_X$ and its complementary stiffness matrix $\mathbf{K}_C$. The links of the robot were assumed to be much stiffer than the joints. Because the stiffness model and, as a consequence, joint stiffness identification become simple when $\mathbf{K}_C$ is negligible with respect to $\mathbf{K}_\theta$, we determined the robot configurations that minimized the influence of $\mathbf{K}_C$ on $\mathbf{K}_X$. The robustness of the method was also studied with a sensitivity analysis of the results to measurement errors and to the number of experimental tests. Moreover, the proposed methodology will be improved in a future work that will identify the link stiffness in addition to the

joint stiffness of industrial robots. Finally, experimental tests will be performed to validate the proposed method.

References

[1] Xuan XF. Optimal pose trajectory planning for robot manipulators. Mechanism and Machine Theory 2002;37:1063–86.
[2] Kim T, Sarma S-E. Toolpath generation along directions of maximum kinematic performances a first cut at machine-optimal paths. Computer-Aided Design 2002;34:453–68.
[3] Matsuoka S-I, Shimizu K, Yamazaki N, Oki Y. High-Speed end milling of an articulated robot and its characteristics. Journal of Materials Processing Technology 1999;95:83–9.
[4] Pan Z, Zhang H, Zhu Z, Wang J. Chatter analysis of robotic machining process. Journal of Materials Processing Technology 2006;173:301–9.
[5] Nagata F, Hase T, Haga Z, Omota M, Watanabe K. CAD/CAM-based position/force controller for a mold polishing robot. Mechatronics 2007;17:207–16.
[6] Zhang H, Hang H, Wang J, Zhang G, Gan Z, Pan Z, et al. Machining with flexible manipulator: toward improving robotic machining performance. In: Proceedings of the 2005 IEEE/ASME international conference on advanced intelligent mechatronics, Monterey, California, USA, July, pp. 24–28.
[7] Nawratil G. New performance indices for 6R robots. Mechanism and Machine Theory 2007;42:1499–511.
[8] Kucuk S, Bingul Z. Comparative study of performance indices for fundamental robot manipulators. Robotics and Autonomous Systems 2006;54:567–73.
[9] Mansouri I, Ouali M. A new homogeneous manipulability measure of robot manipulators, based on power concept. Mechatronics 2009;19:927–44.
[10] Kim BH, Yi BJ, Oh SR, Suh IH. Non-dimensionalized performance indices based optimal grasping for multi-fingered hands. Mechatronics 2004;14:255–80.
[11] Lecerf-Dumas C, Furet B, La Robotique au service de l Entreprise: Nécessité de mai\widehattriser le comportement des robots, Conférence Journée Robotique et Composite, Plate-forme technologique Automatismes et Composites, 2009.
[12] Pashkevich A, Chablat D, Wenger P. Stiffness analysis of overconstrained parallel manipulators. Mechanism and Machine Theory 2009;44:966–82.
[13] Östring M, Gunnnarsson S, Norrlöf M. Closed-loop identification of an industrial robot containing flexibilities. Control Engineering Practice 2009;11:291–300.
[14] Abele E, Weigold M, Rothenbücher S. Modeling and identification of an industrial robot for machining applications. Annals of the CIRP 2007;56(1).
[15] Chen S-F. The 6×6 stiffness formulation and transformation of serial manipulators via the CCT theory. In: IEEE international conference on robotics & automation, Taiwan, 2003.
[16] Khalil W. Dombre E. Modeling, identification and control of robots. Hermes Science Publications, 2002.
[17] Angeles J, Caro S, Khan W, Morozov A. The design and prototyping of an innovative Schönflies motion generator. Proceedings of the IMechE Part C, Journal of Mechanical Engineering Science, special issue: Kinematics Kinematic Geometry and their applications 2006;220(7):935–44.
[18] Golub GH, VanLoan CF. Matrix computations. Baltimore: The Johns Hopkins University Press; 1989.
[19] Angeles J. Fundamentals of robotic mechanical systems theory, methods, and algorithms. 3rd ed. New York: Springer; 2007 (first edition published in 1997).
[20] Li Z. Geometrical consideration of robot kinematics. The International Journal of Robotics and Automation 1990;5(3):139–45.
[21] Paden B, Sastry S. Optimal kinematic design of 6R manipulator. The International Journal of Robotics Research 1988;7(2):43–61.
[22] Khan WA, Angeles J. The kinetostatic optimization of robotic manipulators: the inverse and the direct problems. ASME Journal of Mechanical Design 2006;128:168–78.
[23] Chen S-F, Kao I. Conservative congruence transformation for joint and Cartesian stiffness matrices of robotics hands and fingers. The International Journal of robotics Research 2000;19:835.
[24] Alici G, Shirinzadeh B. Enhanced stiffness modeling, identification and characterization for robot manipulators. IEEE Transactions on Robotics 2005;21(4):554–64.